NUREG/CR-1122
ORNL/NUREG/TM-364
Dist. Category R7

Contract No. W-7405-eng-26

Engineering Technology Division

DEVELOPMENT OF AN ULTRASONIC IMAGING SYSTEM TO MEASURE THE SIZE AND VELOCITY OF LARGE BUBBLES RISING THROUGH LIQUIDS

L. Adler
D. Fitting
J. Lattimer
A. L. Wright

Manuscript Completed - March 24, 1980
Date Published - April 1980

Prepared for the U.S. Nuclear Regulatory Commission
Office of Nuclear Regulatory Research
Under Interagency Agreements DOE 40-551-75 and 40-552-75

NRC FIN No. B0121

Prepared by the
OAK RIDGE NATIONAL LABORATORY
Oak Ridge, Tennessee 37830
operated by
UNION CARBIDE CORPORATION
for the
DEPARTMENT OF ENERGY

Contents

DEVELOPMENT OF AN ULTRASONIC IMAGING SYSTEM TO MEASURE THE SIZE AND VELOCITY OF LARGE BUBBLES RISING THROUGH LIQUIDS

L. Adler*,† J. Lattimer*
D. Fitting* A. L. Wright‡

ABSTRACT

A real-time ultrasonic imaging system was developed to permit the simultaneous measurement of the radii and velocities of large bubbles rising through a liquid. It was constructed as a possible technique for studying the dynamics of large bubbles rising in liquid sodium. The characterization of such bubbles is one part of a program at the Oak Ridge National Laboratory known as the Fuel Aerosol Simulant Test (FAST). The purpose of the FAST program is to investigate events following a simulated hypothetical core-disruptive accident in a liquid-metal fast breeder reactor.

The accuracy and limitations of the system were determined by evaluating the rise of a variety of solid and air-filled spherical test targets in water. Diameters of the test spheres ranged from 3.3 to 24.1 cm; magnitudes of the rise velocities ranged from ~40 cm/s to ~1 m/s. The uncertainty in radii measurements within the interval from 3.3 to 9.10 cm was estimated to be within ±7% at a 95% confidence level. Theoretical calculations of the rise velocities were compared with the measurements performed using the ultrasonic dynamic imaging (UDI) system. In addition, independent experimental measurements of the rise velocities were obtained with a laser-photocell system. Based on those comparisons, the uncertainty in velocity measurements, at a confindence level of 95%, was estimated to be within ±17%. That estimate was made based on the sphere size measured using the UDI system.

1. INTRODUCTION

The work described in this document deals with the development of an ultrasonic imaging system to measure simultaneously the size and velocity of large bubbles rising through a liquid. Such a bubble-sensing technique is needed to characterize bubbles produced in experiments that are part of the Fuel Aerosol Simulant Test (FAST) program being performed at the Oak Ridge National Laboratory (ORNL). This program is part of the Aerosol Release and Transport (ART) program sponsored by the Division of Reactor Safety Research of the Nuclear Regulatory Commission.

The FAST experiments[1] use the ORNL-developed capacitor discharge vaporization (CDV) technique to put samples of uranium dioxide (UO_2) into the high energy states that could be encountered in Liquid-Metal Fast Breeder Reactor (LMFBR) hypothetical core-disruptive accidents (HCDAs). In such accidents, a vapor bubble could be produced which could carry radionuclides through the liquid sodium coolant. These radionuclides would constitute a potential source for release to the atmosphere and the general public. The objective of the FAST experiments, then, is to study the formation, rise, and condensation of a fuel vapor bubble.

*The University of Tennessee, Department of Physics.
†Metals and Ceramics Division.
‡Engineering Technology Division.

The facility for these experiments is depicted in Fig. 1. The test vessel is ~183 cm (6 ft) high and ~61 cm (2 ft) in diameter and is made of 1.9-cm-thick (0.75-in.) 304H stainless steel. The test unit is inserted through one of the lower ports, and liquid levels as high as 112 cm (44 in.) are produced. The initial series of tests will be done using water as the coolant (to permit movies of bubble motion to be taken), but the final series will use liquid sodium. Pressure in the argon gas space above the coolant will be varied between 0.101 and 2.02 MPa (1 and 20 atm).

Greater than 2 g of UO_2 is expected to be vaporized by capacitor discharge. Bubbles containing this much vapor are likely to be spherical caps rather than spheres and to be as large as 30.5 cm (1 ft) in diameter. Rise velocities for bubbles of this size are on the order of 1 m/s.

The major instrumentation problem for the FAST experiments is related to tracking bubbles produced under sodium. The difficulty of these measurements is enhanced by the fact that sodium

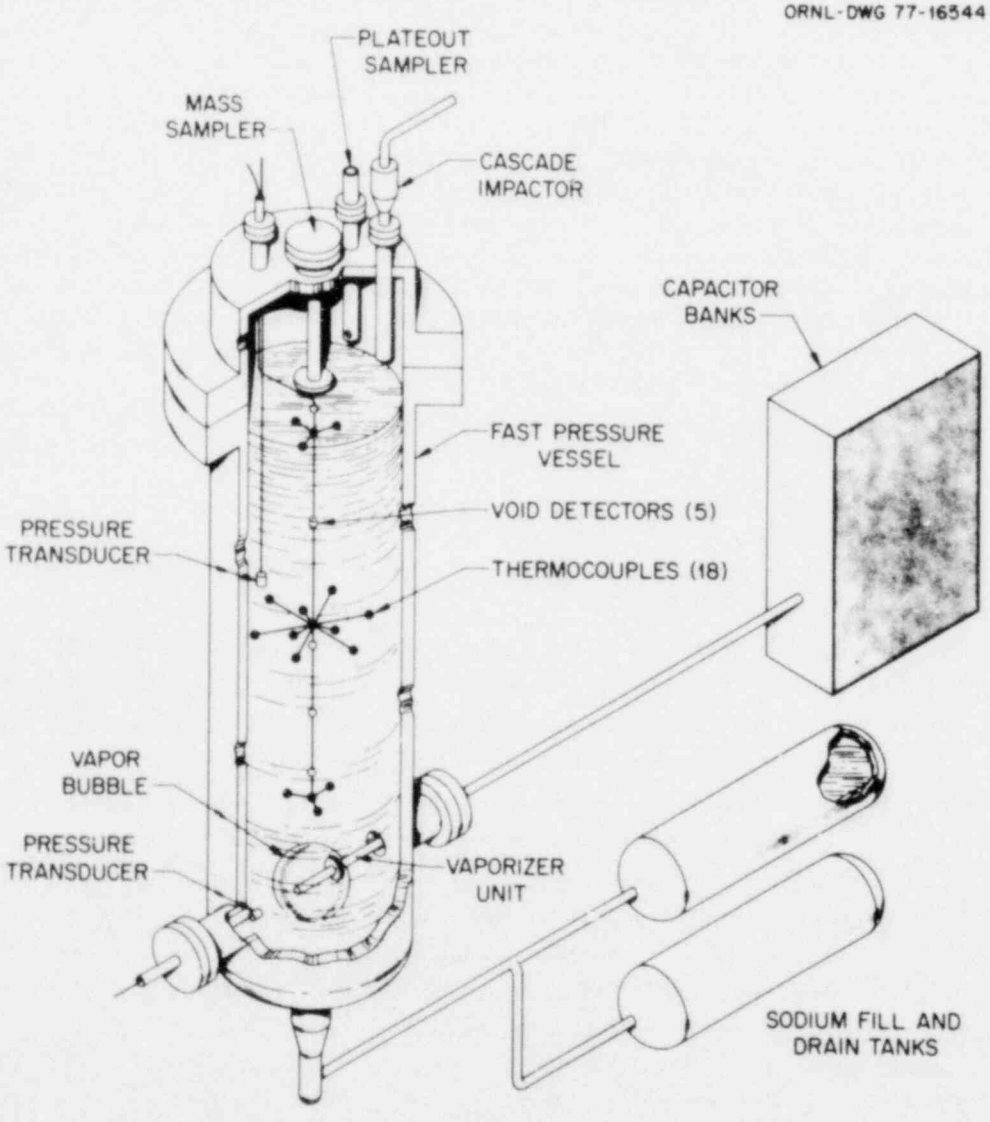

Fig. 1. Fuel Aerosol Simultant Test (FAST) Facility.

temperatures for the tests will be ~866 K (1100° F). Design parameters for any "viewing" system for use in the FAST experiments, then, are as follows.

1. The system must be capable of tracking bubbles rising through an 866 K sodium pool.
2. The most important measurement needed is that of bubble size vs time during rise. The sensing system must be able to measure bubble sizes as large as 30.5 cm (1 ft) and as small as 2.54 cm (1 in.) in diameter.
3. If possible, the system should be capable of measuring bubble rise velocities on the order of 1 m/s.
4. So as not to perturb the motion of the bubble through the coolant, sensing instrumentation should be outside the test vessel (e.g., mounted on the vessel wall).

This problem is within the general realm of problems considered in nondestructive evaluation (NDE); however, it is of a more specialized nature than the typical problems encountered in NDE. A more typical problem in NDE might be the detection and characterization of a small static flaw or inclusion in an otherwise homogeneous material. The present experimental problem, in contrast, has two rather interesting aspects which not only characterize the nature of the problem but also point toward a possible experimental approach to a solution. First, the problem is dynamic—the characterization of the voids in motion. The second characteristic that makes this problem somewhat unique is the large size of the voids. To describe the relationship between the bubble size and ultrasonic parameters, the following definitions are made:

D = diameter of bubble,

λ = wavelength of ultrasound in the liquid,

B = diameter of ultrasonic beam.

In terms of these parameters, the bubble sizes are characterized by the relationships

$$D \gg \lambda$$

and

$$D \gg B .$$

In NDE there are two widely used techniques employing ultrasonics for determining the sizes of flaws and inclusions.[2] First, there are scattering techniques that are used to determine geometrical features such as size and shape from the details of the ultrasonic scattered fields. Second, there are imaging techniques that produce ultrasonic images by displaying echoes in a two-dimensional pattern, which maintains the spatial relationships between the various interfaces and acoustical impedance discontinuities producing the echoes.[3] The dimensions of the voids are much larger than both the ultrasonic wavelength and the beam size, which indicates that imaging is the preferred experimental approach to determining the parameters of the voids.[2]

The potential usefulness of ultrasonics in LMFBR applications has been recognized for some time. The most efficient operation of liquid-metal-cooled reactors requires that techniques be developed

which allow the inservice inspection of reactor components under liquid sodium. Several countries have been actively engaged in the development of suitable inspection techniques for a number of years.[4]

Rohrbacher and Batholamay[5] developed and conducted water tests on an ultrasonic system using A-scan techniques (pulse-echo technique) which could be used for the inspection of fuel elements and the monitoring or scanning of mechanical components under liquid sodium.

An ultrasonic-level measurement system capable of continuously monitoring the sodium level has been tested in sodium at temperatures up to 288° C (550° F).[6]

An ultrasonic under-sodium viewing and ranging system has been developed as a possible in-service inspection method for an LMFBR.[4,7] This system operates in two modes: viewing and ranging. The viewing mode makes use of an imaging technique called IsoScan, which permits high-resolution visualization of objects in three dimensions. Also, dimensions of the object may be measured from a viewing screen using conventional intensity mode displays. Use of the ranging mode permits the location of objects under sodium. This system has been tested in liquid sodium at temperatures up to 260° C (500° F), which is typical of the temperature during reactor shutdown and refueling. The system, however, cannot be used at the normal LMFBR operating temperature of 593° C (1100° F) until suitable high-temperature transducers are developed.

A somewhat similar ultrasonic inspection system having more limited imaging capabilities has been developed in France[4] and used during reactor refueling operations.

All the ultrasonic inspection systems described have at least one of the following characteristics that prevents their use in the study of HCDA bubble dynamics:

1. They are not real-time systems.

2. They have an amplitude mode presentation or similar ranging capability that does not provide suffficient information for the evaluation of bubble parameters without elaborate signal processing.

Numerous investigations were made using acoustical techniques for the general study of bubbles in liquids.[8-12] These investigations, most of which were statistical in nature, dealt with the basic dynamics of bubbles and the interaction of sound with bubbles. They also dealt with the extraction of data from large bubble populations and not with the acoustical probing of single large bubbles. Consequently, the techniques employed in these investigations are not applicable to the investigation described here.

In Germany, an ultrasonic system has been developed which is more closely related to the present investigation.[5] It is a continuous-wave ultrasonic system designed to detect bubbles in liquid sodium. The system was designed to be just a bubble detector; therefore, it does not have the capability of determining the bubble parameters needed to characterize their behaviors.

The most basic physical process encountered in this investigation was the interaction of a pulsed ultrasonic beam with a large moving spherical discontinuity in a liquid. Freedman[13,14] developed a theory pertaining to a mechanism of high-frequency acoustic echo formation that possibly offers some insight into the nature of various phenomena observed in the present investigation.

According to Freedman's theory, high-frequency acoustic echoes returning from a rigid body immersed in an ideal fluid medium may be shown to be composed of a number of discrete pulses. The envelope of each echo pulse closely resembles the envelope of the transmitting pulse, and, therefore, they are called image pulses. An image pulse is formed at a point where a discontinuity exists in $d^n W / dr^n$ with respect to the range r; W refers to the solid angle subtended at the transducer by the portion of the scattering body within a range of r, and n may vary from zero through any positive integer.

The application of Freedman's theory to the echo structure from a rigid sphere is illustrated in Fig. 2, in which the range is considered to be great enough that $Kr_1 \gg 1$, where K is the wave number equal to $2\pi/\lambda$, with λ the pulse wavelength. Discontinuities in d^nW/dr^n occur at the near (r_1) and far (r_2) limits of irradiation. For an acoustic transmission pulse that is sufficiently short, the echo consists of two separately resolved image pulses formed at r_1 and r_2. The echo formed at the near point (r_1) is most relevant to this investigation.

This report describes the preliminary development of an ultrasonic dynamic imaging (UDI) system for use in the FAST experiments. The first step in development of this measurement system was to determine if accurate measurements of bubble parameters could be made by interpreting the output from a single acoustic transducer that beams a signal at a rising bubble. We recognized early in this investigation that the final system for use in FAST would consist of an array of transducers; this would permit the surface of the bubble to be "mapped" by the transducer output. However, the first step necessary was to make measurements using a single transducer, with the transducer signal beamed at the bubble centerline.

In this report, the method of determining bubble size and velocity from acoustic measurements is described. The "bubbles" used in the measurements reported were spheres with diameters ranging from 3.3 to 24.1 cm. Detailed measurements of sizes and velocities for spheres with diameters in the range of 3.3 to 9.1 cm are reported. The size measurements were compared with actual measured sizes; velocities were compared with theoretical predictions and with additional measurements using a laser-photocell system. The accuracy of the measurements and capabilities of the acoustic measuring system are discussed.

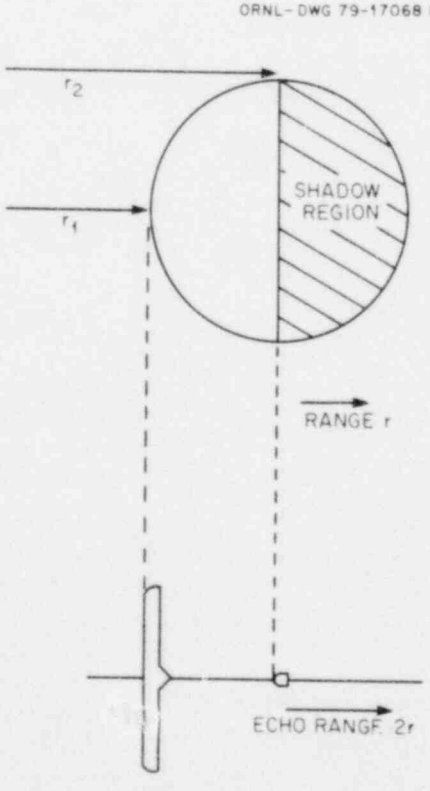

Fig. 2. Echoes from rigid sphere (relative scale used is approximate).

2. EXPERIMENTAL APPARATUS AND PROCEDURES

The experimental work done in this investigation can be divided into three major areas: (1) developing the experimental ultrasonic bubble detection system, (2) testing the performance of the system, and (3) determining the system's limitations, accuracy, and reliability.

2.1 General Description of Experimental System and Its Operation

A real-time ultrasonic system was developed which simultaneously measures the radius and velocity of spherical bubbles rising in liquids; this system will be called the UDI system.

The UDI system and the tank with a mounted transducer are shown in Fig. 3, while Fig. 4 shows the various components of the system in a block diagram. The ultrasonic pulser-receiver provides the radio frequency (rf) excitation to a focused transducer, which is coupled to the outside of a cylindrical test tank filled with water. The transducer, operating in a pulse-echo mode, produces an ultrasonic pulsed beam that traverses the diameter of the tank. A bubble or spherical object passing through the beam produces a back-scattered echo that is received by the same transducer. The signal from the transducer passes through the receiver section of the pulser-receiver, through an amplifier, and into a discriminator. The purpose of the discriminator is to eliminate or drastically reduce the influence of low-level noise on the system. For a signal level below threshold, the discriminator output is zero. The echo from a bubble or object in the beam produces a signal level larger than threshold, and the discriminator output is high. The applied signal then passes to the z-axis of a storage oscilloscope, where the signal modulates the brightness of the scope display. Two independent time bases control the sweep rate along the horizontal and vertical axes of the oscilloscope. The horizontal sweep rate is fast (typically 10 to 50 μs/cm), and the vertical sweep rate is comparatively slower (typically 50 to 100 ms/cm).

The basic principle behind the operation of the UDI system is illustrated in Fig. 5. As the edge of the spherical object or bubble moves through the sound beam, the received echo produces a signal that ultimately arrives at the z-axis of the oscilloscope and causes a bright dot to be displayed on the oscilloscope screen. The position of the dot along the horizontal axis of the oscilloscope is directly proportional to the time required for the sound to travel from the point at which the beam intersects the sphere to the transducer. (The point at which the sound beam intersects the sphere will be referred to as the intersection point.) The time interval required for sound to travel from the intersection point to the transducer is similarly proportional to the distance from the intersection point to the transducer. As the sphere moves upward through the sound beam, the position of the intersection point will change continuously due to the curvature of the sphere. Because the electron beam of the oscilloscope is simultaneously swept along the horizontal and vertical axes, the result is a raster image. For a given horizontal line on the scope, the bright dot indicates the position of the intersection point. Each succeeding horizontal line is displayed vertically due to the sweep of the vertical time base. The result is that the position of the intersection point is mapped out over the entire face of the sphere. The map which is displayed on the oscilloscope is the experimental image of the sphere (when the beam passes through the sphere's axis). As shown in Fig. 5, as the sphere passes through the beam, the distance from the transducer to the center of the spherical interface is smaller by one radius than the distance from the transducer to the periphery of the spherical interface. Therefore, there is a time interval Δt between echoes originating at the periphery of the spherical surface as viewed from the transducer and echoes originating from the center of the spherical surface as viewed from the transducer. This time interval Δt is the time required for sound to travel a distance equal to the radius of the sphere. Figure 6 illustrates

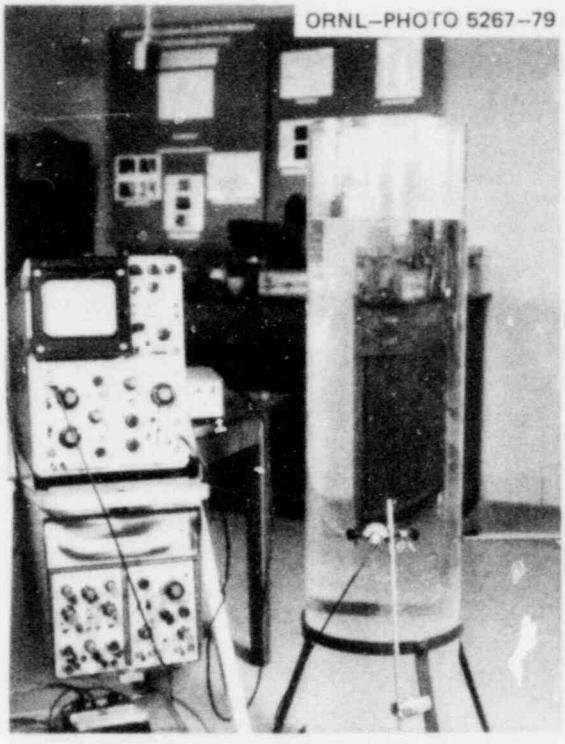

Fig. 3. UDI system and cylindrical test tank.

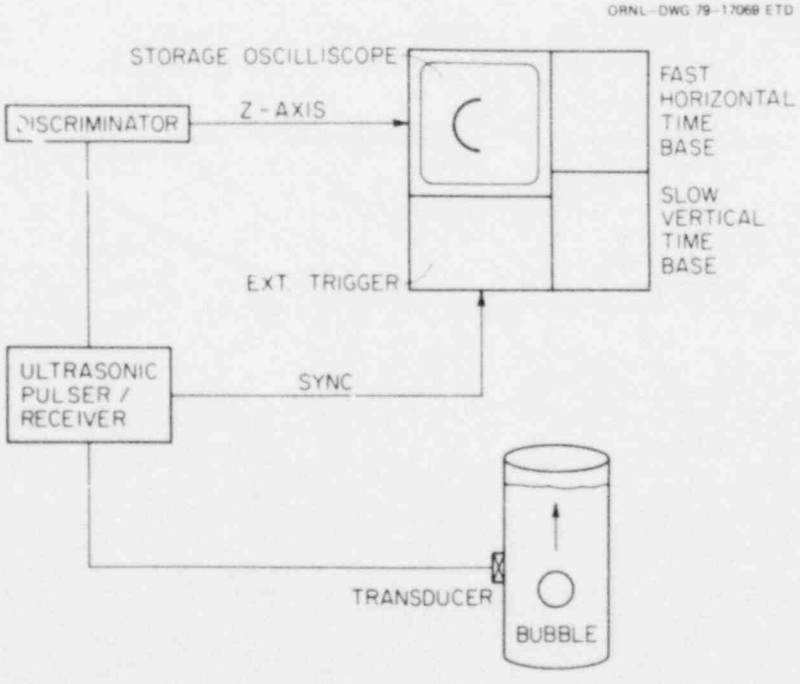

Fig. 4. Ultrasonic dynamic imaging system.

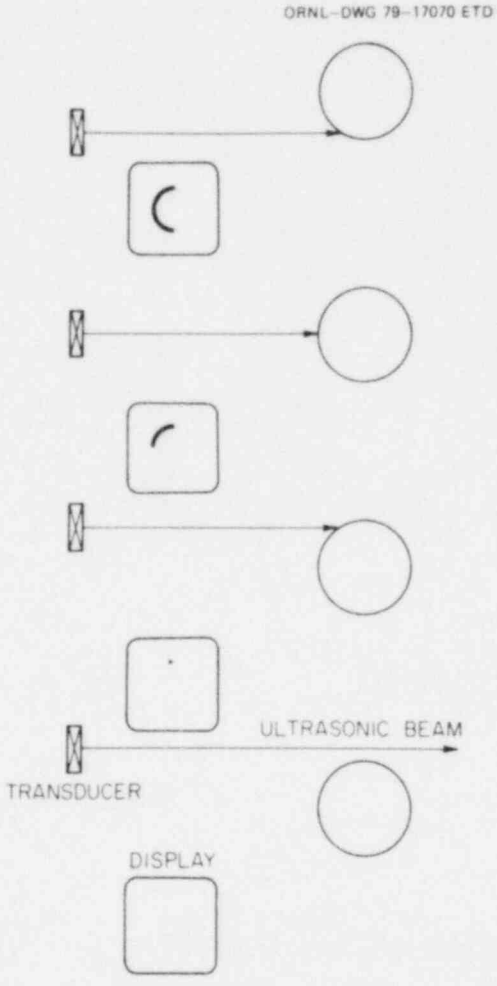

Fig. 5. Demonstration of image formation by the ultrasonic dynamic imaging technique.

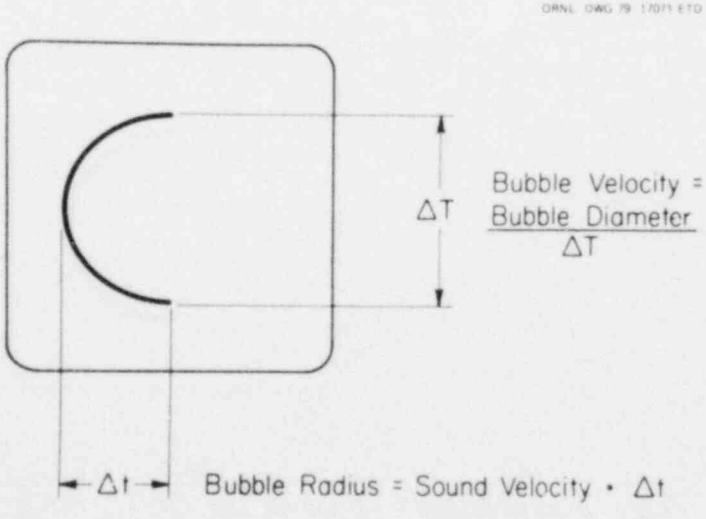

Fig. 6. Simultaneous determination of bubble radius and velocity from profile formed by UDI system.

the resulting trace or image on the oscilloscope. The interval Δt is determined from the horizontal dimension of the trace and the calibrated horizontal sweep rate. The assumption is that the velocity of sound in the liquid is known. Therefore, the radius of the sphere is determined from

$$r = c\,\Delta t\,,$$

where

r = radius of sphere,

c = speed of sound in the liquid,

Δt = (width of the UDI trace)(horizontal time per centimeter setting).

The velocity of the spherical object through the liquid may also be determined using the UDI system when the motion of the sphere is perpendicular to the sound beam and the center of the sphere passes through the center of the beam. If the sphere passes through the beam in a time interval Δt, then the velocity of the sphere is the distance travelled by the sphere in that time divided by time Δt. Therefore, velocity is determined from

$$\text{velocity of sphere} = \frac{\text{diameter of sphere}}{\Delta T}$$

Figure 6 shows that ΔT is determined from the vertical dimension of the oscilloscope trace and the calibrated vertical sweep rate. The diameter is obtained from the horizontal dimension of the trace, as previously described.

In summary, if the velocity of sound in the liquid is known and if the horizontal and vertical sweep rates for the oscilloscope are calibrated, then all of the information needed to evaluate both size and velocity is obtained from the dimensions of the UDI image. Figure 7 shows two images of moving spheres made with the UDI system, together with top and side views of the relative positions of the transducer tank and sphere.

2.2 Detailed Specifi ations of UDI Components

The transducer used for all the experimental work was a commercially made ceramic immersion transducer with a focused beam. It was manufactured by Megasonics (Model ILT). The frequency was 2.25 MHz, the diameter of the transducer was 1.27 cm (0.5 in.), and the focal length was 11.4 cm (4.5 in.).

The pulser-receiver used in the system was manufactured by Panametric Inc. (model 5052PR). In this experiment, the instrument was always used in the pulse-echo mode of operation. The receiver portion of model 5052PR is a 20- or 40-dB amplifier. Coarse and fine attenuators provide stepwise attenuation of the signal to the receiver. When used with the UDI system, the receiver amplifier gain was always set at 40 dB, while the attenuation setting ranged from 20 dB for echoes from very large objects to 0 dB for echoes from the smallest objects. The damping control of the Panametric unit varies the resistance load presented to the transducer by the pulser-receiver. The damping resistance was found to have a significant effect on the quality of the image obtained with the UDI system. The damping

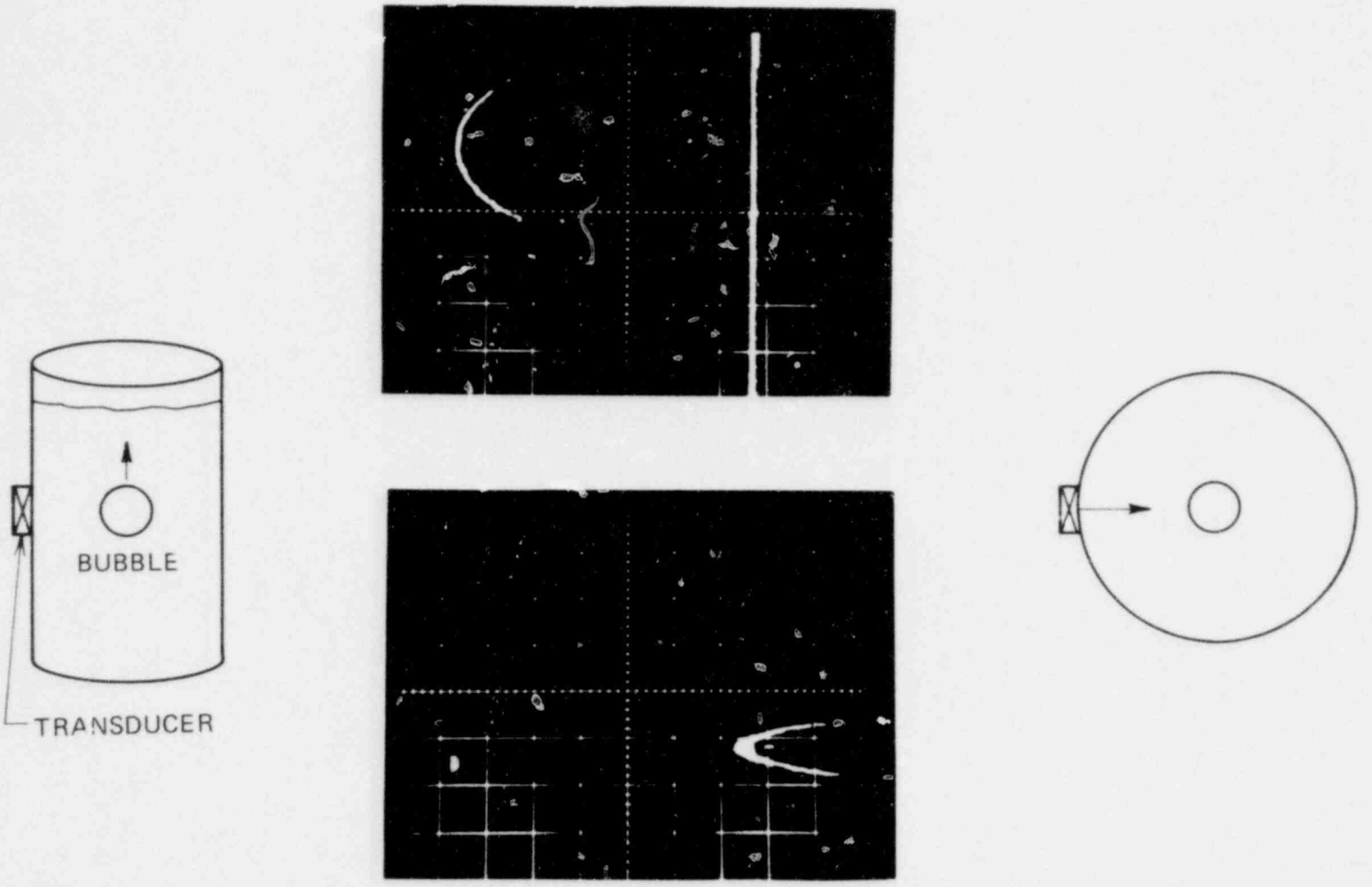

Fig. 7. Side and top views of FAST mock-up and profile of moving spherical discontinuities.

resistances used in the operation of the system ranged from 100 to 175 Ω. Figures 8(a) and (b) are oscilloscope traces showing the echo pattern from a stationary 9.1-cm ball immersed in water.

The amplifier used in the experiment, which was manufactured by Hewlett-Packard (model 465A), is a very low-noise amplifier with voltage gains of 20 or 40 dB. In the UDI system, the amplifier was always used with a gain of 40 dB. The manufacturer lists the frequency response as less than 2 dB down in the range from 5 Hz to 1 MHz; but, in practice, the amplifier was found to have a reasonable gain well beyond 1 MHz.

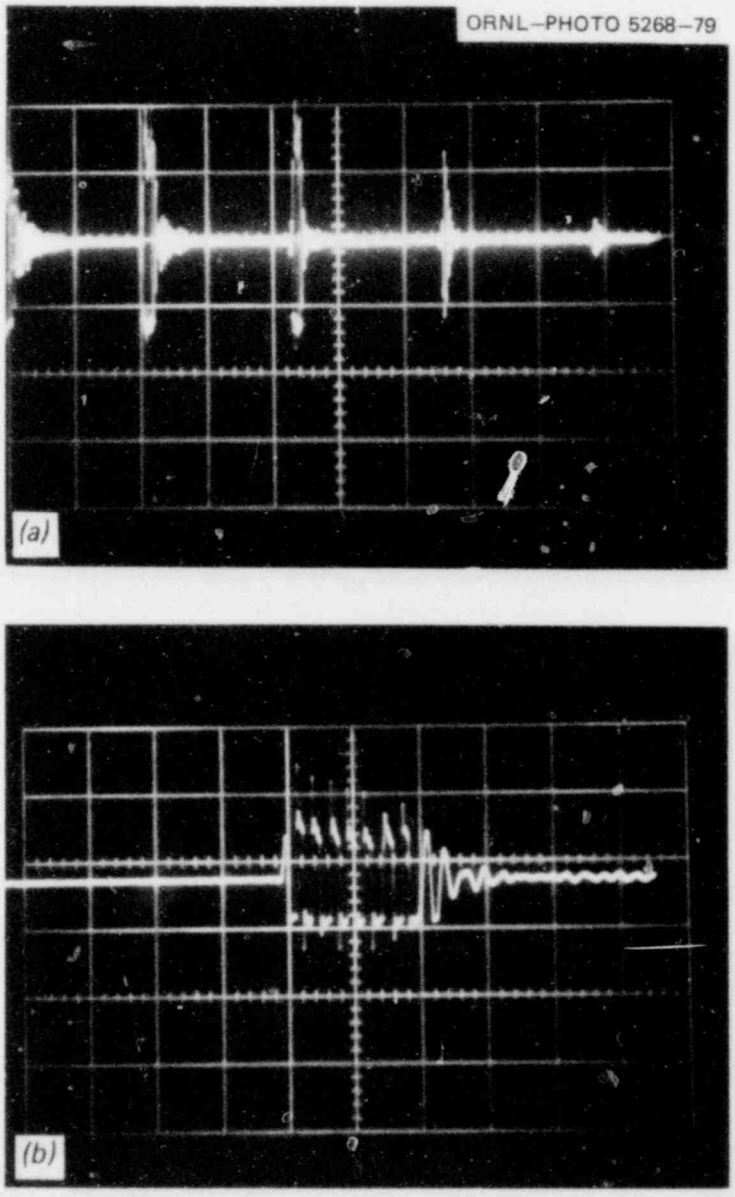

Fig. 8. Echoes from stationary rubber sphere immersed in water. (a) Echo pattern from stationary 9.1-cm solid rubber ball immersed in water (time/cm = 20 μs/cm; V/cm = 1 V/cm); (b) first echo from 9.1-cm rubber ball on expanded time scale (time/cm = 2 μs/cm; V/cm = 2 V/cm).

Figure 9 is a schematic diagram of the discriminator circuit. The transistor acts as a switch. With no signal input or a small signal input, the transistor remains nonconducting with a high resistance, and no trace occurs on the oscilloscope. A large positive signal input turns on the transistor; that is, the transistor is conducting with a relatively small resistance, and the result is a bright trace displayed on the oscilloscope. The circuit acts as a discriminator because it remains cut off for low-level input signals such as those associated with extraneous noise.

The storage oscilloscope used in the system was a Tektronix model 564B. Horizontal sweep was controlled by a conventional time base on the storage oscilloscope; vertical sweep was obtained by feeding a claibrated sawtooth voltage or ramp into the vertical input of the storage oscilloscope. The vertical sensitivity and position controls on the storage scope were adjusted until vertical sweep took place just between the lines defining the boundary of the graticule on the cathode ray tube. The ramp voltage was obtained from the sawtooth output terminal on a Tektronix 555 oscilloscope. The calibrated sweep rate for the ramp had to be multiplied by a correction factor of 1.25 because the vertical sweep on the storage oscilloscope was 8 cm instead of the ramp's 10-cm calibrated sweep length.

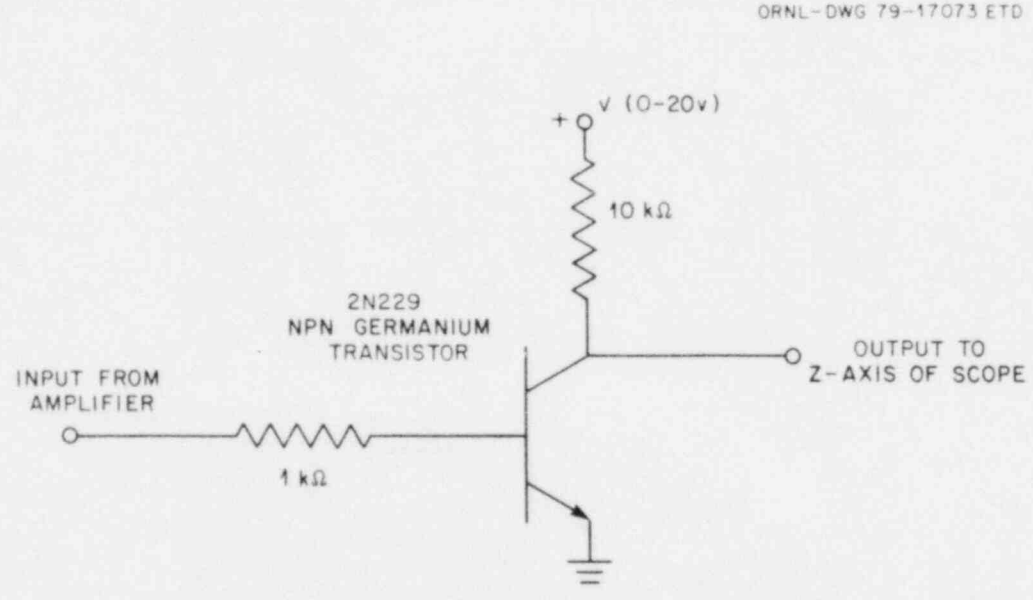

Fig. 9. Schematic diagram of discriminator circuit.

2.3 Preliminary Testing Under Conditions Simulating FAST Experiments

The UDI system was designed to be used in the FAST experiments. A discussion of the FAST operating conditions and the resulting demands placed on the design of any ultrasonic system was presented in Chap. 1. Therefore, the first preliminary tests were made to establish the feasibility of using the UDI system to obtain reasonable results under conditions simulating the FAST experiments.

A mock-up of the FAST facility was prepared for these tests. As discussed in Chap. 1, bubble parameters must be determined with transducers located along the sides of and outside the FAST vessel. Therefore, this series of tests was made using the transducer coupled to the outside of the cylindrical test tank. A clear acrylic tank was used so the interior of the tank could be visually or

photographically monitored. In this series of tests, as well as all other tests described in this work, water was used as the substitute for liquid sodium; in addition, all tests were conducted at room temperature. Disregarding the high-temperature aspects of the FAST experiments, a reasonably close simulation of the FAST experimental acoustic conditions was made possible because of the similarity between the acoustic properties of water and those of liquid sodium. Referring to Table 1, the density and velocity of sound in liquid sodium are reasonably close to the corresponding values for water. Thus, the acoustic impedances of the two liquids are also similar, and, therefore, the acoustic scattering from discontinuities in the two liquids is also approximately the same. The obvious advantages to using water for preliminary testing and development have been exploited not only in this investigation but also in other similar investigations.[1,4,5]

Table 1. Acoustic properties of liquid sodium and water

Property	Material	
	Liquid sodium [593° C (1100° F)]	Water [20° C (68° F)]
Density, kg/m^3	808.2[a]	998.2[b]
Velocity of sound, m/s × 10^3	2.266[a]	1.482[c]
Acoustic impedance, kg/m^2-s × 10^6	1.831[d]	1.479[d]

[a]Ref. 15.
[b]Ref. 16.
[c]Ref. 17.
[d]Calculated values.

Also, for this series of tests, water was used to acoustically couple the transducer and tank. Water was used only for convenience; a number of other substances could have been used for coupling with no apparent effect on the performance of the experiment. As a prelude to high-temperature work, the behavior of a high-temperature coupler called High Tempo 1000 was tested at temperatures up to 93° C (200° F). [According to the manufacturer, KE Aerotech, this coupler should remain stable at temperatures up to 538° C (1000° F).]

A large number of solid and air-filled rubber balls of various sizes were used to simulate bubbles rising vertically through the tank. Such an approach seems reasonable; the signal should be stronger from an air bubble than a rubber sphere.

The cylindrical test tank used in these tests was made of clear acrylic plastic. The outside diameter of the tank was 33 cm (13 in.), with a wall thickness of 0.95 cm (⅜ in.); the length of the cylinder was 129.5 cm (51 in.). The bottom consisted of an acrylic disk bonded to the cylinder, and the tank sat in a steel framework, which acted as a support.

Test balls were released from rest and allowed to rise vertically through the tank. Data taken include the dimensions of the resulting UDI image on the oscilloscope. Collected data were used to calculate the experimentally predicted size and velocity of the test balls. Predicted radii were compared with the actual sizes of the various balls, and experimental velocities were compared with the predicted theoretical velocities for spherical objects rising in water.

2.4 Independent Experimental Check of Velocities

The series of preliminary tests made with the cylindrical plastic tank demonstrated the feasibility of using the UDI system to study the dynamics of spherical objects rising in liquids. The next series of tests was designed to establish the limitations of the system and its accuracy and reliability. Size limitations and limited accessibility of the interior of the cylindrical tank made the various experimental parameters needed to precisely determine the system's exact capabilities difficult to control. Therefore, the remainder of the tests was performed in a more spacious rectangular tank.

In the preliminary tests, experimental velocities were compared with theoretical predictions (presented in Appendix A) of the velocity of spherical objects in water. To more completely determine the accuracy of the velocity predictions obtained with the UDI system, an independent experimental check of the velocities should also be performed. The system used to make independent experimental evaluations of the velocity is shown in Fig. 10. Figure 11 is a block diagram of the experimental laser-photocell system. The method used to determine velocities with the optical system was very similar to the ultrasonic method employed by the UDI system. In the laser-photocell system, the very narrow light beam from a laser was substituted for the ultrasonic beam used in the UDI system; a photocell was similarly substituted in place of the ultrasonic transducer. Referring to Fig. 11, the light beam from the laser passes through the rectangular test tank and strikes a photoelectric cell. The dc signal from the photocell then passes through an amplifier and into the vertical input of a storage oscilloscope. A test ball passing through the laser beam produces a trace such as that shown in Fig. 12. The horizontal width of the oscilloscope trace yields the time interval $\Delta\tau$ required for the ball to pass through the laser beam. In a manner similar to that used with the UDI system, the velocity is calculated as the diameter of the sphere divided by the time interval $\Delta\tau$ required for the sphere to pass through the laser beam.

The laser used in the otpical system was a 0.5-MW helium-neon laser that produced red light of wavelength 6328 Å. The photocell, a selenium-coated photoelectric cell, was mounted in an aluminum

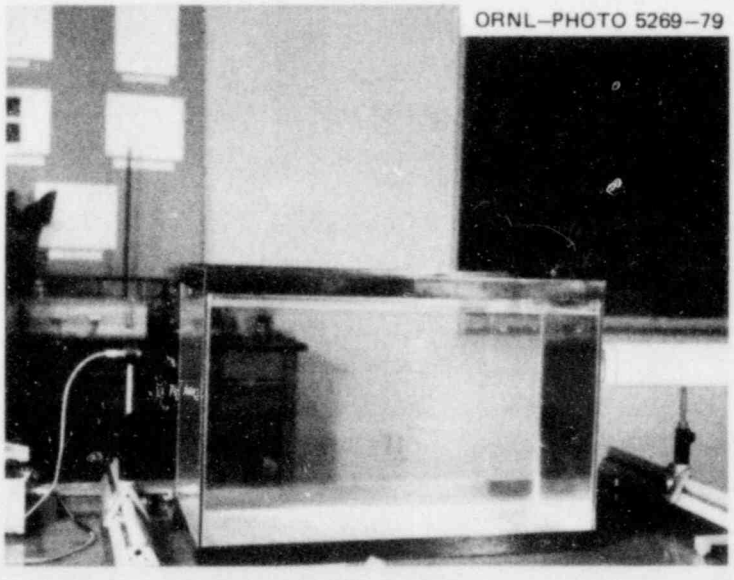

Fig. 10. Laser-photocell system used to experimentally check UDI velocity measurements.

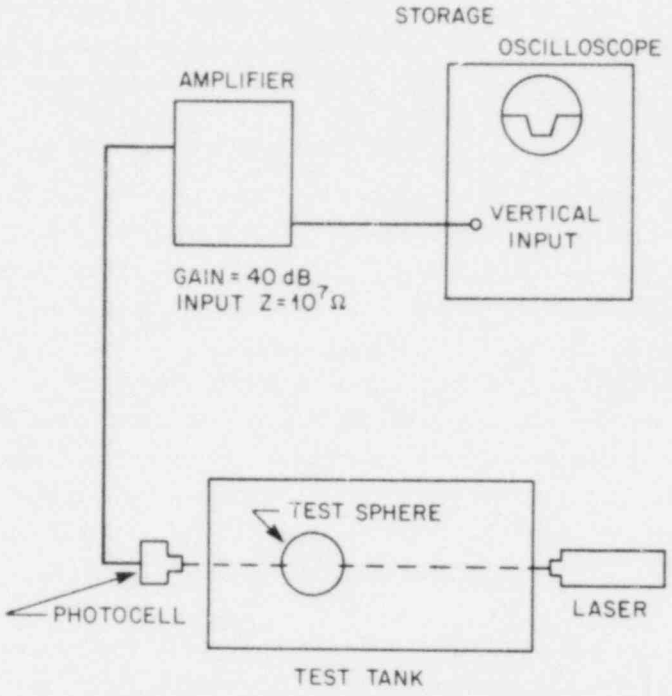

Fig. 11. Block diagram of laser-photocell optical system.

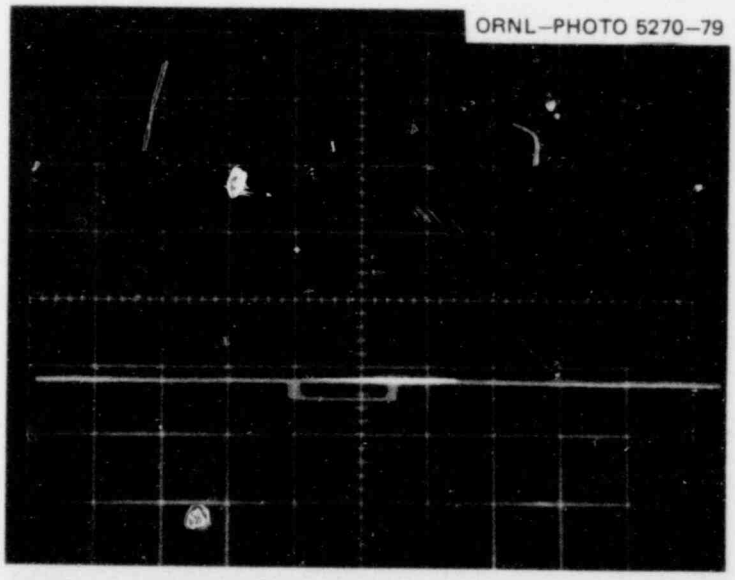

Fig. 12. Typical trace obtained using laser-photocell system to monitor motion of spherical test target.

canister 2.54 cm (1 in.) in diameter. A circular opening with the same approximate dimension as the laser beam was located in the center of the canister. The laser light entered through the opening and struck the photosensitive element approximately 1.3 cm (0.5 in.) behind the opening. The amplifier used in the system, which was constructed in the Physics Department at The University of Tennessee for general laboratory use, was built with a field-effect transistor (FET) operational amplifier as the active component in the device. The amplifier had voltage gains of 0, 20, 40, and 60 dB. The input impedance could be varied from 10^3 to $\infty\Omega$.

In using the optical system to take velocity data, an adjustable stand was placed inside the test tank. The height of the stand was used to vary the distance the test balls traveled from rest before intersecting the laser beam. In each case, an adjustment was made allowing the center of the test balls to travel a distance of 14 cm from rest on passing through the laser beam. All test balls used in this series of tests were solid rubber. The horizontal time scale on the oscilloscope ranged from 20 to 50 ms/cm. Input impedance to the amplifier was $10^7\Omega$, and the gain was 40 dB.

The accuracy of this method for determining velocities depended on how closely the center of the test spheres passed through the center of the laser beam. In practice, the alignment of the sphere's center with the laser beam could be monitored closely by visually observing the laser beam as it cut across the ball passing through the beam. Data for those attempts that were visually judged to be off center were rejected. The time interval for each test ball was recorded in a data run of 20 attempts. The mass of the ball was measured prior to and after each data run to ensure that the mass had not changed due to the absorption of water.

The sides of the trace were observed to be slightly sloped in some instances. This effect was minimized by reducing the depth of the trace. The method used for the data was to measure the time interval $\Delta\tau$ as the full width at half minimum.

2.5 Procedure for Investigation of UDI System's Limitations, Accuracy, and Reliability

For reasons previously stated, most of the final exhaustive testing of the UDI system's capabilities was made in the rectangular test tank. The experimental setup is illustrated in Figs. 13 and 14. The transducer used in these tests was the same one previously described. However, instead of being coupled to the outside of the tank, the transducer was immersed inside the tank. The same adjustable stand described in the previous section was used to vary the distance the test spheres traveled from rest. Outside the tank, the laser's position was adjusted so that the laser beam struck the center of the transducer parallel to the ultrasonic beam. The laser beam served as a visual reference line for determining whether the test spheres passed through the center of the sound beam. As described in the previous section, the data were rejected for those attempts that were visually judged to be off center. The distance the spheres traveled from rest was adjusted to 14 cm to correlate with velocity data obtained using the laser-photocell system. Prior to using the system for a data run with a particular test sphere, first determining the optimum settings for the attenuation and damping controls on the pulser-receiver was found expedient. A data run was made for each different test sphere. Whenever feasible, the horizontal distance from the transducer to the center of the sphere was chosen to be close to the focal length of the transducer. (A more detailed discussion of this parameter is given in Chap. 3.) Each data run typically consisted of from 15 to 25 passages of the test sphere through the ultrasonic beam. The UDI oscilloscope image yielded the previously described time intervals ΔT and Δt, which were then used to calculate the radius and rise velocity for that particular test sphere.

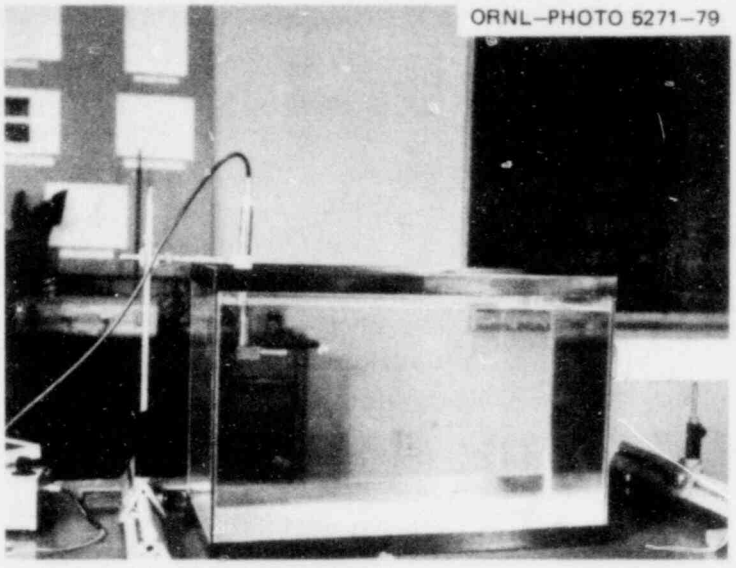

Fig. 13. Experimental setup used for testing UDI system.

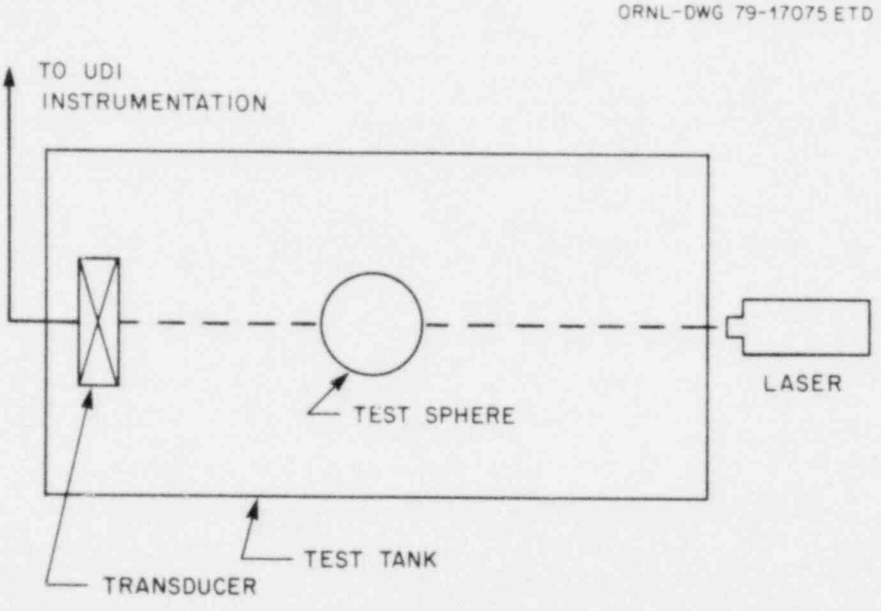

Fig. 14. Diagram of setup used to test UDI system.

The temperature of the laboratory was thermostatically controlled at a reasonably constant temperature of 20° C. The value used for the velocity of sound in distilled water at 20° C and 1 atm was 1482.92 m/s, as determined by Wilson.[17]

Experimental size measurements were compared with the known size of the test sphere, and percentage errors were calculated. The experimental results for velocity were compared with (1) the velocity predicted theoretically for a spherical object moving in water and (2) the velocity measured using the laser-photocell method.

A wide variety of test spheres was used to investigate the limitations of the UDI system's velocity predictions. By using both air-filled and solid balls of different sizes and compositions, the velocity of the test objectives could be varied from a few centimeters per second to several meters per second. This variation of velocity was found to be large enough to allow a determination of the approximate range within which the UDI system functioned accurately.

The limitations of the system's ability to accurately determine size were investigated in a similar manner. The response of the system was monitored over a wide range of sizes for the test spheres.

Testing of the UDI system was carried out as described in the rectangular test tank for test spheres having diameters up to 9.1 cm. Spheres larger than this were tested in a large plastic drum filled with water. The physical limitations imposed by the available space in the laboratory made using a test tank larger than this impractical, and the nature and size of this test tank also made measuring the velocity of the largest spheres impractical. Therefore, no velocity information was obtained for the 24.1-cm ball. However, some measurements of radius were made by retarding the ball's motion in the tank.

The raw experimental data from UDI and laser-photocell measurements are presented in Appendix B.

3. RESULTS AND DISCUSSION

3.1 Discussion of Preliminary Tests

With the transducer coupled to the outside of the cylindrical acrylic tank, test balls were released at all points along the interior diameter of the tank. The results of these tests showed that a usable UDI image could be obtained from any point along a diameter coinciding with the sound beam and that the UDI system could be used to monitor the size and motion of spheres intersecting the sound beam anywhere within the tank.

In the next test series, a comparative study was made to determine whether there were any differences in the UDI image obtained from different types of test targets (air-filled or solid spheres). A detailed comparison of the resulting experimental data indicated that there were no apparent differences in the basic nature of the UDI images obtained from the different test targets.

Additional investigations were made comparing the UDI images obtained under the following conditions:

1. the test sphere was released within the cylindrical tank, and the transducer was coupled to the outside of the tank;
2. the transducer and sphere were both located within the rectangular test tank.

The results of the study indicated that there were no basic differences in the shape or dimensions of the UDI image obtained in the two different cases; however, the ultrasonic signal was more attenuated on passing through the walls of the cylindrical tank. As a result of this attenuation, obtaining a usable UDI image was more difficult when the smaller test targets were located at the farthest point from the transducer.

3.2 Experimental Determination of Size

Referring to Table 2, the experimental results for the radii measurements obtained with the UDI system are listed as a mean value, and the experimental uncertainties are indicated in the form of the standard deviation calculated for each data sample. The total number of observations comprising a data sample for a particular test sphere is also indicated in Table 2. A comparison of the calculated mean values and the actual radii is presented as a percentage error. The percentage errors ranged from 0 to 7.8%. In six of seven cases, the percentage error was less than 5%, and in three of the seven cases, the percentage error was less than 2%. The techniques of statistical inference were used to predict more realistically the total uncertainty in the experimental results for the determination of size. Using the data sample for each particular test sphere, the method of confidence intervals[18,19] was used to obtain a predicted range for the population mean at a 95% confidence level. (This is described in Appendix C.) Results of these calculations are listed in Table 3. Experimental radii measurements are expected to lie within the indicated intervals with a certainty of 95%. Boundaries of the predicted intervals were then compared with the actual value of the particular radius to estimate the range of expected uncertainties. Referring to Table 3, the estimated uncertainty for the case of the 12.05-cm-radius sphere was particularly large. However, as previously indicated in Chap. 2, the practical difficulties encountered in measurements with this large target made it necessary to limit the data sample to only seven observations. Therefore, the estimated uncertainties associated with these data samples may not necessarily represent the system's capabilities. Because of this, an evaluation of the system's

Table 2. Radii measurements obtained with UDI system

Actual radius (cm)	Observations in data sample	Radius predicted by UDI techniques[a] (cm)	Error comparison between experimental and actual radius (%)
1.63	15	1.63 ± 0.15	0.0
2.21	20	2.30 ± 0.15	4.1
2.44	15	2.63 ± 0.14	7.8
2.75	20	2.85 ± 0.12	3.6
3.10	20	3.14 ± 0.17	1.3
4.55	25	4.60 ± 0.37	1.1
12.05	7	11.5 ± 1.7	4.6

[a]Plus or minus one standard deviation.

Table 3. Statistical predictions of range for experimental radii at 95% confidence level

Actual radius of test sphere (cm)	Statistical predictions of range for experimental radii at 95% confidence level (cm)	Resulting range of uncertainty (%)	
		Lower limit	Upper limit
1.63	1.63 ± 0.08	5.1	5.1
2.21	2.30 ± 0.07	0.89	7.2
2.44	2.63 ± 0.08	4.6	11.0
2.75	2.85 ± 0.06	1.6	5.6
3.10	3.14 ± 0.08	1.1	3.9
4.55	4.60 ± 0.15	2.3	4.4
12.05	11.5 ± 1.6	8.5	17.5

performance is made for the range of test spheres having diameters from 3.26 to 9.10 cm. Within this range of sizes, the total estimated uncertainty in the determination of size was within ±7%.

Referring to the results in Table 2, observe that the experimentally predicted radii were either larger than or equal to the actual radii in all cases except one. This fact indicates the presence of a possible systematic error in the determination of size. This conjecture is further substantiated by the results presented in Table 3; in three of the seven cases presented in Table 3, the total predicted size range for the experimental radii was greater than the actual radii. Furthermore, we observed independently during the process of taking data that there was a tendency for the horizontal dimension of the UDI image to appear too large. No connection was apparent between this observed trend in the data and the calibration and adjustments of the instrumentation. The trend appears to indicate an intrinsic characteristic of the UDI technique itself; however, within the range of sizes considered in this investigation, this is apparently not a serious source of uncertainty.

Another similar factor that appeared to have some influence on the accuracy of the experimental measurement of radii was the relative position of the center of the test ball and the focal point of the sound beam. Whenever feasible, the test spheres were positioned so that their centers corresponded to

the focal point of the sound beam. No detailed investigation was made to determine the quantitative effect of the relative position of the ball and the focal point on the overall accuracy of the radii measurements. However, we observed in a qualitative manner that when the test balls passed very close (2 to 3 cm) to the transducer, the experimental prediction of size was somewhat larger than the actual size. Beyond a range of 2 to 3 cm from the transducer, this factor was not observed to have any noticeable effect on the determination of size.

The positions of the attenuation and damping controls on the pulser-receiver acted as a perturbing effect on the determination of size because too much attenuation of the signals caused the trailing segment of the UDI image to be clipped off. Generally, the attenuation of signals was one of the most serious sources of uncertainty and the one which was least capable of being controlled.

3.3 Experimental Determination of Rise Velocity

The rise velocities of the test spheres were measured with the UDI system and compared with (1) the theoretical results presented in Appendix A and (2) the independent experimental velocity predictions obtained with the laser-photocell system. The experimental velocities measured with the UDI system are listed in Table 4, and the experimental velocities measured using the laser-photocell system are listed in Table 5. In both cases, the experimental results are stated as a mean value, and

Table 4. Experimental velocities measured with UDI system

Diameter of test sphere (cm)	Observations comprising data sample	Velocity measured with UDI system (cm/s)[a]
3.26	15	46.7 ± 3.7
4.41	19	63.3 ± 3.7
4.88	15	75.5 ± 4.2
5.50	20	85.3 ± 3.5
6.20	20	89.8 ± 3.9
9.10	25	104.0 ± 7.2

[a]Plus or minus one standard deviation.

Table 5. Experimental velocities measured with laser-photocell system

Diameter of test sphere (cm)	Observations comprising data sample	Velocity measured with laser-photocell system (cm/s)[a]
3.2	20	44.8 ± 2.7
4.41	20	58.8 ± 2.8
4.88	20	65.6 ± 2.1
5.50	20	79.2 ± 1.8
6.20	20	80.8 ± 2.2
9.10	20	100.3 ± 2.0

[a]Plus or minus one standard deviation.

uncertainties are expressed as the standard deviation for the data sample. The number of observations comprising each data sample is also listed in Tables 4 and 5.

Results obtained using the two independent experimental methods are presented in Table 6. They are compared on the basis of a percentage difference. Table 7 lists the results obtained using the UDI system and the results of the theoretical calculations presented in Appendix A. A comparison of the experimental with the theoretical results is made by means of a percentage error. Finally, the laser-photocell velocity predictions are compared with the theoretical velocity predictions in Table 8.

A further comparison of the velocities obtained with the UDI and laser-photocell systems was made using the methods of statistical inference. A statistical prediction was made for the range of differences between the mean velocities obtained using the two independent experimental methods, with the predicted range of differences calculated at a 95% confidence level.[18,19] The range of differences in the mean velocities was then used to calculate a predicted range for the percentage difference in each case. Results of those calculations are listed in Table 9. In a similar manner, the techniques of statistical inference were used to obtain a 95% confidence level prediction of the expected range in mean velocities obtained with the UDI system. This predicted range in experimental velocities was then compared with the theoretical velocities, and a resulting range of percentage errors was calculated. Results of those calculations are listed in Table 10.

Table 6. Comparison of velocities obtained using UDI system and laser-photocell system

Diameter of test sphere (cm)	Velocity obtained with UDI system (cm/s)[a]	Velocity obtained with laser-photocell system (cm/s)[a]	Difference (%)
3.26	46.7 ± 3.7	44.8 ± 2.7	4.2
4.41	63.3 ± 3.7	58.5 ± 2.8	7.9
4.88	75.7 ± 4.2	65.6 ± 2.1	14.3
5.50	85.3 ± 3.5	79.2 ± 1.8	7.4
6.20	89.8 ± 3.9	80.8 ± 2.2	10.6
9.10	104.0 ± 7.2	100.3 ± 2.0	3.6

[a]Plus or minus one standard deviation.

Table 7. Comparison of experimental UDI velocity measurements with theoretical velocity predictions

Diameter of test sphere (cm)	Velocity obtained with UDI system (cm/s)[a]	Theoretical predictions of velocity (cm/s)	Difference (%)
3.26	46.7 ± 3.7	48.9	4.5
4.41	63.3 ± 3.7	65.2	2.9
4.88	75.7 ± 4.2	70.6	7.2
5.50	85.3 ± 3.5	85.4	0.1
6.20	89.8 ± 3.9	84.9	5.8
9.10	104.0 ± 7.2	106.7	2.5

[a]Plus or minus one standard deviation.

Table 8. Comparison of experimental laser-photocell velocity measurements with theoretical velocity predictions

Diameter of test sphere (cm)	Velocity obtained with laser-photocell system (cm/s)[a]	Theoretical velocity predictions (cm/s)	Difference (%)
3.26	44.8 ± 2.7	48.9	8.4
4.41	58.8 ± 2.8	65.2	10.2
4.88	65.6 ± 2.1	70.6	7.1
5.50	79.2 ± 1.8	85.4	7.3
6.20	80.8 ± 2.2	84.9	4.8
9.10	100.3 ± 2.0	106.7	5.9

[a]Plus or minus one standard deviation.

Table 9. Statistical prediction of range of differences in mean velocities measured with UDI system and laser-photocell system (at 95% confidence level)

Diameter of test sphere (cm)	Predicted range of differences between mean velocities (cm/s)		Resulting range of differences (%)	
	Lower limit	Upper limit	Lower limit	Upper limit
3.26	0	3.8	0	8.3
4.41	3.0	6.6	4.9	10.8
4.88	8.2	12	11.6	17.0
5.5	4.6	7.6	5.6	9.2
6.2	7.2	10.6	8.4	12.4
9.1	0.9	6.5	0.9	6.40

Table 10. Statistical prediction of range of rise velocities measured with UDI system at 95% confidence level

Diameter of test sphere (cm)	Statistical prediction of UDI velocity range (cm/s)	Resulting range of errors (UDI velocity compared with theoretical velocity) (%)	
		Lower limit	Upper limit
3.26	46.7 ± 1.8	0.8	8.5
4.41	63.3 ± 1.5	0.6	5.4
4.88	75.7 ± 1.9	1.3	12.4
5.5	85.3 ± 1.4	3.9	4.3
6.20	89.8 ± 1.5	3.9	7.3
9.10	104.0 ± 2.5	0.2	5.0

Based on comparison of the UDI velocities with the independent laser-photocell data and the theoretical velocity predictions, the estimate is that, with a confidence level of 95%, the total experimental uncertainty in the determination of velocity is within ±17%. The velocity measurement relies on measurement of the sphere size, which in itself was uncertain with ±7%. This means that the additional measurement (in addition to size) needed to measure rise velocity has a ±10% uncertainty associated with it.

A comparison of the standard deviations obtained from the UDI data with those obtained from the laser-photocell data (Tables 4 and 5) indicates that a substantially greater random error is present in the UDI measurements. This result, however, is to be expected from the basic nature of the probing beams used in the two different methods. The laser beam is a very narrow well-collimated beam in contrast to the much larger focused ultrasonic beam.

A factor contributing to uncertainties in the velocity data obtained from both the UDI and the laser-photocell systems was the occasional irregular lateral motion of the less massive test balls. The absence of this lateral motion in the case of the much more massive 9.1-cm ball may have contributed to the very close agreement between the different velocity measurements obtained for this ball.

3.4 UDI System's Reliability and Limitations

There appears to be a lower limit to the size of spherical objects which can be accurately and reliably measured using UDI techniques. This lower limit has been determined experimentally to be ~3.0 cm in diameter for the system used in this investigation. Some sizing information was obtained for objects having diameters smaller than 3.0 cm; however, in those cases, either the predicted sizes were less accurate or the actual UDI image formation was unreliable. The existence of a lower limit in the determination of size is to be expected as the dimension of the target approaches the diameter of the beam used to probe the target. This lower limit could probably be reduced by using different transducer diameters and frequencies; however, the present limits are considered compatible with the requirements of the FAST program. The largest test sphere used in this investigation had a diameter of 24.1 cm; to date, no apparent upper bound was observed which limited the experimental determination of size.

The UDI system in its present state measures rise velocities most effectively for magnitudes ranging from a few centimeters per second to 1.5 m/s. The experimental measurement of velocities in the range from 1.5 to 2 m/s was reasonably accurate; however, the UDI image formation was not as reliable. For rise velocities above 2.0 m/s, the UDI image was not defined sufficiently for measurements. A factor that becomes important at higher rise velocities is that the raster image spacing becomes greater at higher vertical sweep rates, and the result is that the resolution of the system is decreased. This decreased resolution affects the accuracy of both size and velocity measurements to some extent. Evidence acquired during this investigation indicates that the relatively poor quality of the storage oscilloscope being used in the present UDI system is one of the major factors contributing to the unreliable responses of the system to large rise velocities. The present state of the system, however, is adequate for use in the FAST program because the expected rise velocities in the FAST experiments correspond approximately to the center of the present range of applicability.

A number of limiting factors are inherent in the design of the system. One example (previously mentioned) is that the UDI system actually measures an average velocity over the time interval required for the sphere to pass through the sound beam. This factor places no limitations on the accuracy of velocity measurements if the velocity is constant. For large accelerations, predicted experimental velocities would deviate significantly from actual instantaneous velocities. The accurate measurement

of instantaneous velocity using UDI techniques therefore is limited to those cases in which either no acceleration occurs or the acceleration is small. Another limiting factor inherent in the design of the system is that the motion of the target sphere must be perpendicular to the sound beam. Any significant lateral motion by the target sphere along the direction of the sound beam either toward or away from the transducer would alter the UDI image.

If all electronic adjustments are optimum, the overall reliability of the UDI system is reasonably good. A usable image is obtained in ~75 to 80% of the total number of observations. Failure to obtain a usable image was usually attributable to the formation of the image at the edge of the oscilloscope screen. In the case of spherical targets, the image is symmetrical; therefore, half the image provides sufficient data for the determination of both radius and velocity.

Thus far, all discussion concerning the accuracy, reliability, and performance of the UDI system has been made with the tacit assumption that the center of the target sphere passed directly through the center of the sound beam. This will not necessarily be the case in the FAST tests, and investigation of the influence of this on measurements is needed.

3.5 Detailed Examination of UDI Image

Some of the features observed in the UDI oscilloscope trace and the resulting treatment of the data require a brief explanation. For smaller test spheres, a close examination of the oscilloscope trace reveals the existence of two different signals, as illustrated in Fig. 15. The segment of the trace appearing to the right in Fig. 15 will be called the main trace; the segment of the trace appearing to the left will be

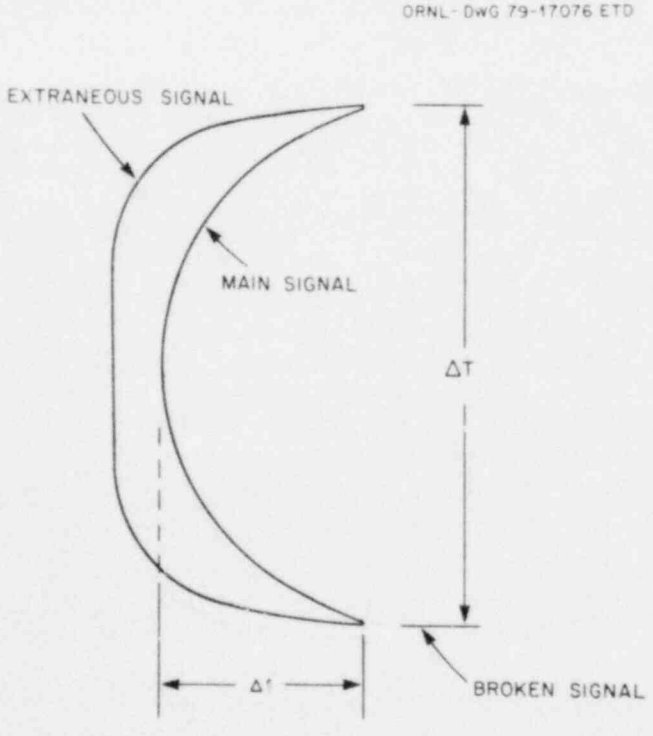

Fig. 15. Composite image.

called the extraneous trace. In the course of this investigation, we established that the main trace yields more accurate time intervals for the determination of both size and velocity.

The extraneous signals were observed for both solid and air-filled targets. Because an ultrasonic signal in the megahertz range is not propagated through air, the extraneous signal likely did not result from multiple reflections within the sphere. Figure 16 illustrates that the extraneous trace became more prominent and more widely separated from the main trace as the size of the test sphere was decreased. The extraneous trace appears to be either missing or to coincide with the main trace for very large test

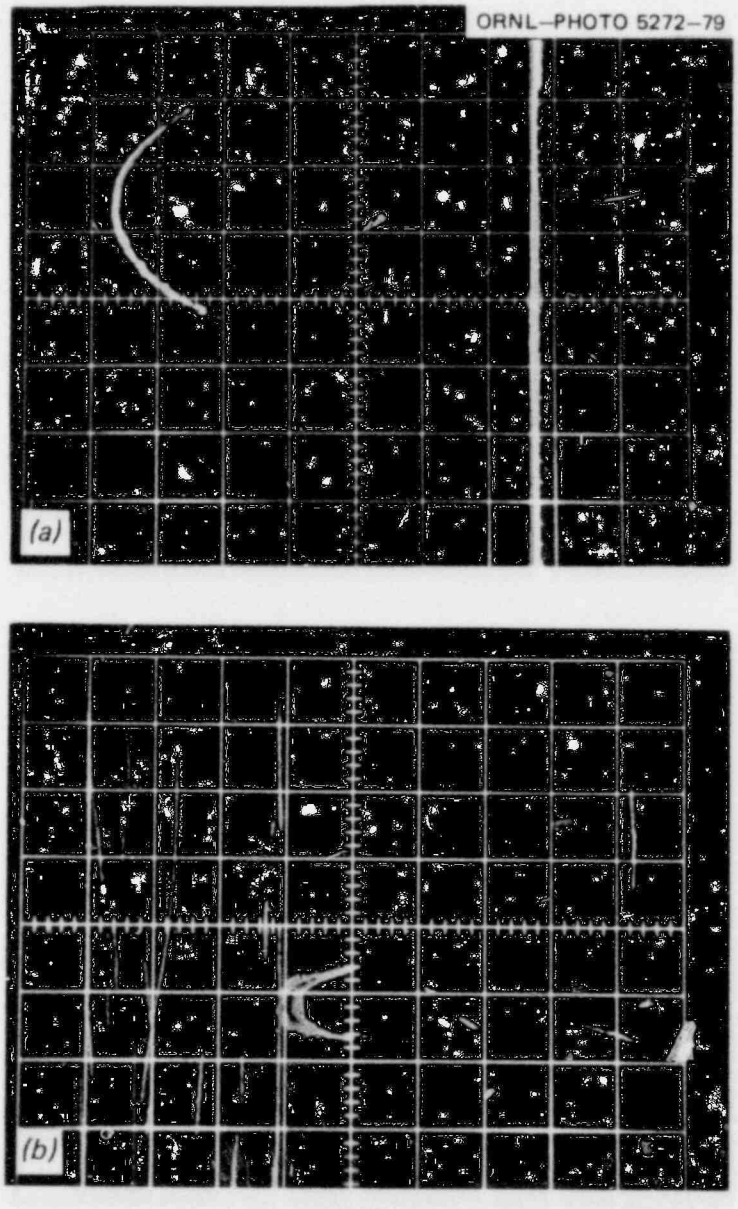

Fig. 16. Comparison of images for small and large test spheres. (a) Image of 24.1-cm-diam sphere. Note apparent absence of extraneous signal (horizontal time scale, 50 μs/cm). (b) Image of 6.2-cm-diam sphere. Note extraneous signal to left (horizontal time scale, 20 μs/cm).

spheres. In some instances, the quality of the image was such that the two components could not be clearly distinguished from each other. In these cases, reasonably accurate predictions of size can be obtained by measuring the time interval Δt from the center of the cresent-shaped image, because the two component traces appear to merge together in the approximate center of the composite trace. In contrast to the size time interval Δt, the velocity time interval ΔT was measured in the usual manner.

In some cases, a series of broken signals was observed trailing from the UDI image. That situation is also illustrated in Fig. 16. The measurement method used in these tests was to measure the horizontal dimension of the image up to the first break.

3.6 Origin of UDI Signals

An effort was made to establish the origin of the UDI signals relative to the various regions of the test sphere. This subject was investigated in the following manner: The focused transducer was immersed in the rectangular tank, and a laser beam was positioned to coincide with the outer perimeter of the sound beam. The same experimental setup was used in this test as that previously described in Chap. 2 of this report. A large semitransparent air-filled plastic ball having a diameter of 18.5 cm served as the test target. The intersection of the sound beam with the test sphere was indicated by the position of the laser beam on the sphere. Using this procedure, ultrasonic signals apparently returned from all portions of the hemispherical segment facing the transducer, including the periphery or outer edge of the sphere. The return of ultrasonic signals from the edge was confirmed when the edge of the sphere was allowed to just graze the sound beam.

At least two different signals returned from the test sphere. The signal originating from the central portion of the sphere was the result of specular reflection. However, the distinctly different signals originating from the outer portions of the sphere could not have resulted from reflection. The existence of a signal returning from the edge of the sphere could possibly be related to the phenomena described by Freedman.[13,14]

4. SUMMARY AND CONCLUSIONS

An ultrasonic imaging system was developed as a possible means of studying the dynamics of large vapor bubbles that are associated with HCDAs in an LMFBR. The study of HCDA-related phenomena is being conducted in the FAST program.

The experimental ultrasonic imaging system, designated the UDI system, is a real-time system which has the capability of measuring simultaneously the radius and the rise velocity of large spherical bubbles rising in a liquid. The system has been used to monitor the motion and size of spherical objects rising through a water-filled acrylic tank having a diameter of 30.5 cm. Spherical test targets having a variety of different sizes and compositions were used to establish the accuracy, limitation, and reliability of the system. Tests were made using spherical targets with diameters ranging from 3.26 to 24.1 cm. For spherical targets with diameters in the range of 3.26 to 9.10 cm, the total experimental uncertainty in the size measurement was estimated to be within ±7%. This estimation was made at a 95% confidence level.

The rise velocities of the same spherical test objects were measured with the UDI system and compared with (1) the theoretical predictions of rise velocity for a sphere in a liquid and (2) independent experimental measurements of rise velocity, both of which were performed with a laser-photocell system. The total experimental uncertainty in the measurement of rise velocity was estimated to be within ±17% at a 95% confidence level. Magnitudes of the measured velocities were within the interval from ~40 to 105 cm/s. These velocity measurements were made using the sphere sizes measured with the UDI system as input.

The lower limit to the reliable measurement of spherical diameters has been placed at 3.0 cm for the present system. There does not appear to be a corresponding upper limit to the size of spherical targets which can be reliably and accurately measured. Evidence indicates that the present system could be used to measure rise velocities most accurately for magnitudes ranging from a few centimeters per second to 1.5 m/s. Measurement of rise velocities greater than 2.0 m/s is not possible with the present instrumentation. Improvements in the instrumentation could greatly increase the range of velocities that can be measured. The basic design of the UDI system limits accurate velocity measurements to those cases in which there is either no acceleration or only a small acceleration. One of the major limiting factors associated with the single-transducer UDI system is the requirement that the center of the target sphere pass through the center of the sound beam. This requirement will make using multitransducer arrays necessary to effectively monitor bubbles in the FAST experiments.

Under optimum conditions, the reliability of the UDI system was such that a usable image was obtained in ~80% of the total observations.

In summary, the single-transducer UDI system has the capability of measuring the size and velocity of spheres that rise in a closed cylindrical container. In addition, the system functioned effectively within the ranges of both size and velocity expected in FAST applications.

5. SUGGESTIONS FOR FURTHER WORK

The following are suggestions for the work necessary to develop the final system needed for the FAST experiments.

1. The preliminary tests described were performed in a cylindrical acrylic test tank. The next logical step in the further development of the UDI system would be a series of water tests, which would be performed in a cylindrical tank made of 304H stainless steel that might have any convenient height; however, the tank should have a diameter of 61 cm (2 ft) and a wall thickness of 1.9 cm (¾ in.) to duplicate the FAST pressure vessel. Such tests would permit the UDI system to be evaluated under conditions very closely simulating the FAST tests and would provide a menas by which the equipment could be calibrated prior to participating in the actual FAST tests.

2. The results presented were obtained using one transducer positioned so that the center of the test spheres passed directly through the center of the sound beam. The accuracy of UDI measurements depends directly on the center of the spherical test objects passing through the center of the sound beam. To effectively monitor the interior of a large cylindrical vessel, using an array of transducers therefore will be necessary instead of using a single transducer. One possible linear array that would cover the cross section of the tank is illustrated in Fig. 17. Other array designs are possible, and a thorough investigation should be made to determine which type of array offers the greatest accuracy and reliability. A multiple array system will probably be needed in the FAST tests. Arrays placed at different heights along the cylindrical pressure vessel would be needed to study the condensation of a bubble as it rises through a sodium pool.

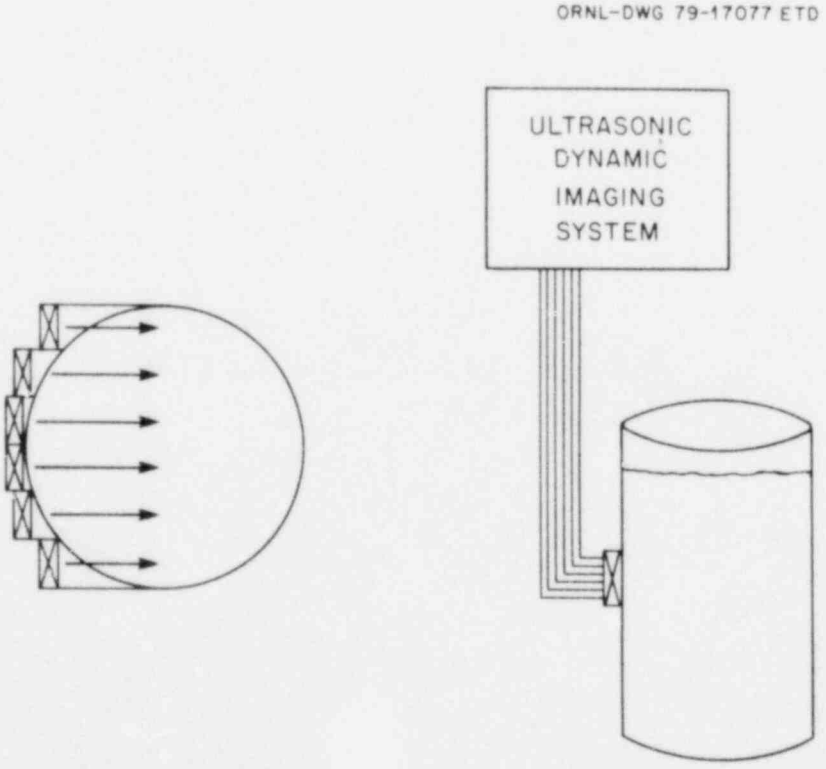

Fig. 17. Linear array of transducers for UDI.

3. Spherical test objects have been used in this investigation because they were easier to control in an exhaustive study of the system's performance. In contrast, however, very large bubbles rising through a liquid will probably assume the shape of spherical caps. Therefore, a follow-on investigation should be made using test objects in the form of spherical caps instead of spheres.

4. Focused transducers have been used thus far in this investigation. Comparing the results obtained with focused and nonfocused transducers having the same frequency and diameter would be useful. Also, a more extensive study must be conducted into the effects on accuracy of the measurements resulting from the relative position of the sound beam focal point and the center of the test object.

5. Although some initial work has been done in this investigation, additional investigation with different frequencies and beam diameters is necessary to obtain an optimum balance between resolution and attenuation.

6. Improvements are needed in the signal processing electronics of the UDI system. The present electronic circuitry, although adequate, could be greatly improved.

7. The use of some electronic signal recording method such as magnetic tapes should be considered. This capability is needed for accumulation of large quantities of data from multiple transducer arrays in the relatively short bubble rise times.

8. Inquiries should be made concerning the possibility of using the various image processing and pattern recognition techniques for the postprocessing of the UDI image data.

9. All the work described in this report was done at room temperature. In contrast, the outside temperature of the FAST pressure vessel will be 593° C (1100° F) during the actual sodium test series. Application at these temperatures must be demonstrated; thus, insulating buffer rods or cooling techniques must be investigated.

10. A more detailed study should be made of the various factors such as multiple signals which contribute to the formation of the UDI image.

ACKNOWLEDGMENTS

This work was performed primarily in The University of Tennessee Department of Physics but also in the ORNL Metals and Ceramics (M&C) Division. We wish to thank R. W. McClung of the M&C Division for the use of division facilities and personnel. Funding for the work was provided through the ORNL Aerosol Release and Transport (ART) Program, sponsored by the Advanced Reactor Safety Research Division of the Nuclear Regulatory Commission through Union Carbide Subcontract 7252, Task Order 2. Our thanks go to T. S. Kress, the ART Program Manager, for supporting this work.

REFERENCES

1. A. L. Wright, A. M. Smith, and T. S. Kress, *Fuel Aerosol Simulant Test (FAST) Plan*, ORNL/NUREG/TM-129 (1977).
2. B. R. Thompson, *Proceedings of the ARPA/AFML Review of Quantative NDE*, p. 33 (1976).
3. R. C. Addison, Jr., *Proceedings of the ARPA/AFML Review of Quantative NDE*, p. 273 (1976).
4. N. C. Hoitink and C. K. Day, *Under-Sodium Viewing System Development for FFTF*, HEDL-TME 75-103 (1975).
5. H. A. Rohrbacher and R. Batholomay, *Ultrasonic Measurement Techniques in Systems Under Sodium*, EURFNR-1255 (1975).
6. L. S. Boehmer, *An Ultrasonic Instrument for Continuous Measurement of Liquid Levels in Sodium Systems*, HEDL-TME 75-137 (1975).
7. C. C. Scott and Shuh-Pan Ying, *Development of the Under-Sodium Ultrasonic Scanner*, Atomic Power Development Associates, Report No. 210 (1967).
8. E. L. Carstensen and L. Foldy, "Propagation of Sound through a Liquid Containing Bubbles," *J. Acoust. Soc. Am.* **19,** 481 (1947).
9. H. Medwin, "Acoustical Determination of Bubble-Size Spectra," *J. Acoust. Soc. Am.* **62,** 1041 (1977a).
10. H. Medwin, "Counting Bubbles Acoustically: A Review," *Ultrasonics* **11** (January 1977b).
11. V. P. Glotov, P. A. Kolobaev, and G. G. Neuimin, "Investigation of the Scattering of Sound by Bubbles Generated by an Artificial Wind in Sea Water and the Statistical Distribution of Bubble Sizes," *Sov. Phys.-Acoust.* **7,** 341 (1962).
12. C. S. Clay and H. Medwin, *Acoustic Oceanography*, John Wiley and Sons, New York, 1977.
13. A. Freedman, "A Mechanism of Acoustic Echo Formation," *Acoustica* **12,** 11 (1962a).
14. A. Freedman, "The High Frequency Echo Structure of Some Simple Body Shapes," *Acoustica* **12,** 62 (1962b).
15. O. J. Foust, ed., *Sodium-NaK Engineering Handbook*, Gordon and Breach, Inc., New York, 1972.
16. R. L. Daugherty and J. B. Franzini, *Fluid Mechanics with Engineering Applications*, McGraw-Hill, Inc., New York, 1977.
17. W. D. Wilson, "Speed of Sound in Distilled Water as a Function of Temperature on Pressure," *J. Acoust. Soc. Am.* **31,** 1067 (1959).
18. W. J. Dixon and F. J. Massey, Jr., *Introduction to Statistical Analysis*, McGraw-Hill, Inc., New York, 1969.
19. M. D. LaMont, L. L. Douglas, and R. A. Oliva, *Calculator Decision-Making Sourcebook*, Texas Instruments, Inc., Dallas, Texas, 1977.

Appendix A

THEORETICAL VELOCITY PREDICTIONS

One of the primary objectives of this investigation was the development of an experimental technique for measuring the rise velocities of spherical discontinuities in a liquid. Predictions of the rise velocities for the spherical test targets used in this investigation were calculated using the theory of fluid mechanics.[16] Figure A.1 illustrates the forces acting on a solid sphere rising in a liquid medium. In Fig. A.1 and in the calculations that follow, motion is assumed to progress in the y direction from an initial state of rest. B refers to the upward buoyant force, W refers to the weight of the sphere, and F_D refers to the total drag force acting on the sphere. The drag force F_D is given by

$$F_D = C_D \rho \frac{AV^2}{2}, \tag{1}$$

where

C_D = drag coefficient,

ρ = mass density,

V = velocity,

A = projected frontal area of the sphere [$A = (\pi D^2)/4$].

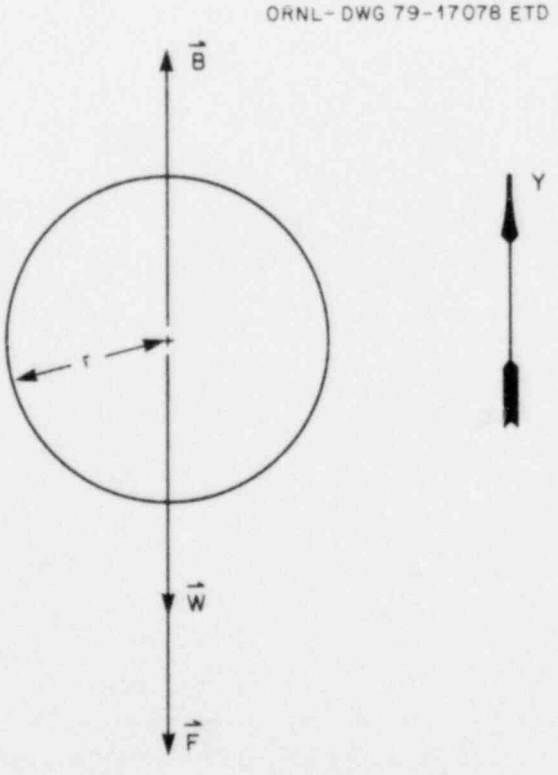

Fig. A.1 Forces acting on sphere rising in liquid medium.

The equation of motion for the sphere is given by

$$m \frac{dV}{dt} = B - W - \frac{C_D \rho A V^2}{2} , \tag{2}$$

where

m = mass,

V = velocity,

t = time.

After redefining the constants and introducing the new variables, Eq. (2) assumes the following form:

$$mV \frac{dV}{dy} = \beta - \gamma V^2 , \tag{3}$$

where

$\beta = B - W$,

$\gamma = \frac{C_D \rho A}{2}$,

$t = \gamma / V$.

The solution to Eq. (3) (assuming C_D = constant) is written as

$$V = \left\{ \frac{\beta}{\gamma} \left[1 - \exp\left(- \frac{2\gamma y}{m} \right) \right] \right\}^{1/2} , \tag{4}$$

with the solution based on these initial conditions: $y_0 = 0$, $V_0 = 0$, $t_0 = 0$. To use Eq. (4) to evaluate the rise velocities, determining the drag coefficients for each test sphere was necessary. Figure A.2 is a plot of the empirical drag coefficients for a sphere as a function of Reynolds number N_R. The Reynolds number for a sphere is defined as

$$N_R = \frac{DV}{\nu} , \tag{5}$$

where

D = diameter of the sphere,

V = velocity,

ν = kinematic viscosity ($\nu = \mu / \rho$) of the liquid.

Pertinent data describing the solid rubber test spheres used in this investigation appear in Table A.1. The kinematic viscosity of water at 20° C was taken as 1.003×10^{-6} m^2/s from Daugherty and Franzini.[16] Experimental velocities measured with ultrasonic techniques were substituted into Eq. (5),

and the resulting Reynolds number was used to obtain the drag coefficients from Fig. A.2. The drag coefficients and the measured parameters of the test spheres were then substituted into Eq. (4). In each case, the theoretical calculations were made with the assumption that the spheres traveled 14 cm from rest to correlate the theoretical data with the experimental data. Results of the theoretical calculations are presented in Table A.2. These theoretical velocity predicitons are compared with the experimentally measured velocities in Chap. 3 of this report.

Table A.1. Description of test spheres

Diameter (cm)	Mass (g)
3.26	14.4
4.41	32.3
4.88	42.5
5.50	54.8
6.20	80.6
9.10	241.8

Table A.2 Theoretical velocity predictions for test spheres[a]

Diameter of test sphere (cm)	Calculated velocity (cm/s)
3.26	48.9
4.41	65.2
4.88	70.6
5.50	85.4
6.20	84.9
9.20	106.7

[a]Distance of travel is 14 cm from rest.

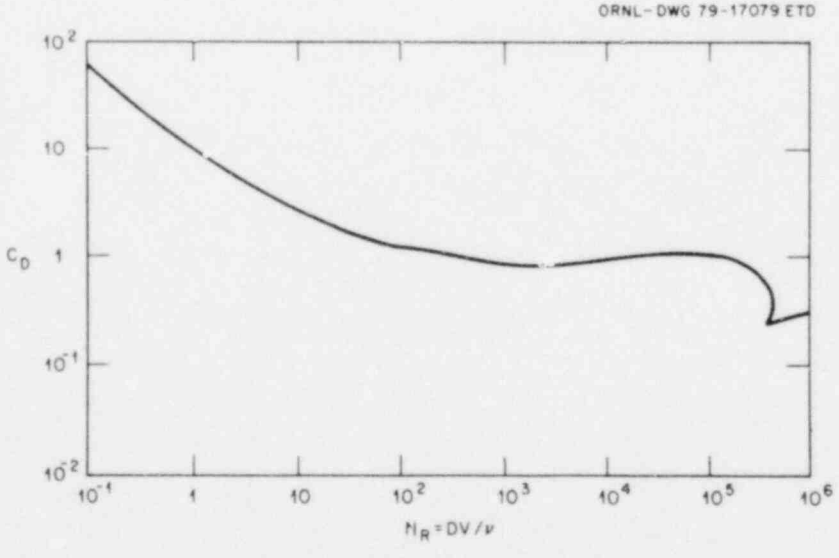

Fig. A.2 Drag coefficients for sphere.

Appendix B

RAW EXPERIMENTAL DATA

A detailed description was given in Chap. 2 of the quantitative tests which were used to establish the accuracy of the UDI system. Data obtained with the UDI system are presented in Table B.1. The independent velocity data obtained with the laser-photocell system are presented in Table B.2. The means and standard deviations of the time intervals obtained with the UDI system are listed in Table B.3, and the corresponding means and standard deviations of the time intervals obtained with the laser-photocell system are presented in Table B.4. In all cases, the data correspond to a distance of travel of 14 cm from rest.

Table B.1. Size and velocity data obtained with the UDI system

Diameter of test sphere (cm)	Δt (μs)	ΔT (ms)	Diameter of test sphere (cm)	Δt (μs)	ΔT (ms)
3.26	12.0	71.9		19.0	65.6
	10.0	68.8		20.0	65.6
	11.0	68.8		19.0	63.1
	10.5	75.0		20.0	68.8
	11.0	68.8		18.0	62.5
	12.6	75.0		19.4	71.9
	10.0	68.8		19.0	65.6
	11.0	75.0		20.0	68.8
	13.0	75.0		20.0	71.9
	12.0	68.8	6.20	22.0	71.9
	11.5	75.0		22.0	71.9
	10.5	59.4		22.0	68.8
	10.0	68.8		20.0	68.8
	10.0	68.8		22.0	71.9
	10.0	62.5		21.0	68.8
4.41	16.0	75.0		20.0	71.9
	16.0	75.0		20.0	68.8
	15.0	71.9		20.0	65.6
	15.0	75.0		22.0	68.6
	14.0	71.9		20.0	65.6
	15.0	71.9		21.0	71.9
	16.4	78.6		22.0	75.0
	15.0	71.9		22.0	71.9
	17.0	75.0		23.0	75.0
	15.0	71.9		19.0	65.6
	16.0	75.0		20.0	71.9
	16.2	73.1		22.0	68.8
	16.4	78.1		23.0	71.9
	15.6	75.0		21.0	65.6
	16.0	76.3	9.10	34.0	90.6
	15.0	71.9		34.0	90.6
	15.0	68.8		34.0	87.5
	14.0	68.8		32.0	90.6
	14.0	71.9		30.0	87.5
	17.6	68.8		32.0	87.5
4.88	18.0	68.8		34.0	90.6
	18.0	68.8		32.0	90.6
	17.0	67.5		30.0	87.5
	16.0	65.6		30.0	87.5
	18.0	68.8		30.0	87.5
	16.6	68.8		30.0	90.6
	18.0	65.6		28.0	87.5
	18.0	75.0		26.0	87.5
	16.0	70.6		36.0	106.25
	19.0	68.8		32.5	93.8
	19.0	70.0		34.0	90.6
	18.0	68.8		30.0	81.3
	18.0	73.8		30.0	86.3
	18.0	70.0		30.0	81.3
	18.0	70.0		30.0	87.5
5.50	18.0	68.8		30.0	81.3
	20.0	68.8		30.0	81.3
	19.0	65.6		27.5	90.6
	19.8	68.8		27.5	88.8
	20.0	65.6	24.1	90.0	No velocity
	19.0	65.6		70.0	data were
	20.4	68.8		65.0	taken for
	18.0	68.8		65.0	this test
	19.8	68.8		90.0	sphere
	18.0	62.5		85.0	
	18.0	62.5		80.0	

Table B.2. Velocity data obtained with the laser-photocell system

Diameter of test sphere (cm)	Δt (ms)	Diameter of test sphere (cm)	Δt (ms)
3.26	80.5	4.88	75.0
	75.0		75.0
	70.2		74.0
	72.5		71.0
	70.2		77.5
	72.5		74.5
	83.5		75.5
	76.0		76.0
	77.5		75.0
	70.5		70.0
	70.0		73.5
	67.5		77.5
	72.5		77.0
	79.0		73.5
	67.5		78.0
	67.5		74.0
	70.0		75.5
	75.0		70.0
	68.5		72.5
	72.5		74.0
4.41	77.5	5.50	67.0
	77.5		67.2
	76.0		69.0
	80.0		69.2
	78.5		65.6
	77.0		69.0
	77.5		69.8
	71.0		69.8
	72.5		70.0
	75.0		69.0
	67.5		69.0
	80.0		70.4
	74.0		71.0
	80.0		69.5
	75.0		72.0
	72.5		69.8
	75.0		70.2
	70.0		69.0
	80.0		71.4
	75.0		71.0
6.20	75.0	9.10	90.0
	71.5		90.0
	76.0		90.5
	77.5		91.0
	76.0		91.0
	75.5		90.0
	77.5		91.0
	78.0		92.5
	73.0		89.5
	78.0		89.5
	79.5		90.0
	76.0		86.0
	80.0		91.5
	78.0		91.0
	77.5		90.0
	77.5		91.5
	78.5		94.5
	77.5		91.0
	77.0		89.5
	76.0		94.0

Table B.3. Means and standard deviations for time intervals obtained with UDI system

Diameter of test sphere (cm)	Δt (μs)	ΔT (ms)
3.26	11.0 ± 1.0	70.0 ± 4.7
4.41	15.5 ± 0.99	73.4 ± 2.9
4.88	17.7 ± 0.91	69.4 ± 2.5
5.50	19.2 ± 0.84	66.9 ± 2.9
6.20	21.2 ± 1.2	70.0 ± 2.9
9.10	30.9 ± 2.5	88.5 ± 5.0
24.1	77.9 ± 11.1	

Table B.4. Means and standard deviations for velocity time intervals obtained with laser-photocell system

Diameter of test spheres (cm)	$\Delta \tau$ (ms)
3.26	76.8 ± 2.0
4.41	75.6 ± 3.6
4.48	74.5 ± 2.3
5.5	69.5 ± 1.52
6.2	76.8 ± 2.0
9.1	90.7 ± 1.8

Appendix C

STATISTICAL CALCULATIONS

The statistical formulas used in Chap. 3 of this report are well known.[18,19]

The predicted range for a population mean was used to obtain the intervals within which both the experimental velocities and the experimental radii were predicted to lie at a confidence level of 95%. The formula used for that calculation is as follows:

$$\text{predicted range for population mean} = \bar{x} \pm \frac{S_x}{\sqrt{n}}\, t\ ,$$

where

$\bar{x}$ = mean value for the sample,

S_x = sample standard deviation,

n = size of the sample,

t = probability t score obtained from the standard statistical tables (at a 95% level of certainty and a degree of freedom equal to $n - 1$).

In a similar manner, the two independent experimental measurements of the velocities were compared by finding the predicted range of differences between population means. Let the subscript H refer to the experimental method that has the higher standard deviation and let L refer to the experimental method that has the lower standard deviation. Initially, an F-test is conducted. The quantity

$$S_{x_H}{}^2 / S_{x_L}{}^2$$

is calculated and compared with the F values obtained from standard statistical tables. If the calculated value is less than the F value listed in the tables, the F-test is passed; otherwise, the F-test is failed. If the F-test is passed, the degree of freedom is given as

$$\text{degree of freedom} = n_H + n_L - 2\ .$$

If, however, the F-test is failed, the degree of freedom is given as

$$1/\{[K^2/(n_H - 1)] + [(1 - K)^2/(n_L - 1)]\}\ ,$$

where

$$K = (S_{x_H}{}^2/n_H)/[(S_{x_H}{}^2/n_H) + (S_{x_L}{}^2/n_L)]\ .$$

The degree of freedom in either of the above cases was used to obtain the t score (at a 95% confidence level) from the statistical tables. The predicted difference between the means was then calculated by

substituting the t value into the following formula:

Range of difference between means

$$= (\bar{x}_H - \bar{x}_L) \pm \{[(n_H - 1)S_{x_H}{}^2 + (n_L - 1)S_{x_L}{}^2][(1/n_H) + (1/n_L)/(n_H + n_L - 2)]\}^{1/2} t \, .$$

NUREG/CR-1122
ORNL/NUREG/TM-364
Dist. Category R7

Internal Distribution

1–5. L. Adler
6. R. S. Booth
7. K. V. Cook
8–12. D. Fitting
13. M. H. Fontana
14. D. Jared
15. T. S. Kress
16. R. C. Kryter
17. R. W. McClung
18. F. R. Mynatt
19. J. L. Rich
20. J. M. Rochelle
21. W. A. Simpson
22. G. M. Slaughter
23. A. M. Smith
24. M. L. Tobias
25. H. E. Trammell
26. D. B. Trauger
27–31. A. L. Wright
32. ORNL Patent Section
33–34. Central Reserch Library
35. Y-12 Document Reference Section
36–37. Laboratory Records Department
38. Laboratory Records (RC)

External Distribution

39–43. J. Lattimer, University of Tennessee, 401 Physics Bldg., Knoxville, TN 37916
44. D. L. Basdekas, Experimental Fast Reactor Safety Research Branch, Division of Reactor Safety Research, Nuclear Regulatory Commission, Washington, DC 20555
45–48. Director, Office of Nuclear Regulatory Research, Nuclear Regulatory Commission, Washington, DC 20555
49. Office of Assistant Manager, Energy Research and Development, DOE, ORO
50–51. Technical Information Center, DOE
52–411. Given distribution as shown in category R7 (NTIS—10)

☆U.S. GOVERNMENT PRINTING OFFICE: 1980-640-245/022